Breather turbulence versus soliton turbulence: Rogue waves, probability density functions, and spectral features

N. Akhmediev,[1] J. M. Soto-Crespo,[2] and N. Devine[1]
[1]*Optical Sciences Group, Research School of Physical Sciences and Engineering, The Australian National University, Canberra ACT 0200, Australia*
[2]*Instituto de Óptica, C.S.I.C., Serrano 121, 28006 Madrid, Spain*
(Received 24 June 2016; published 23 August 2016)

Turbulence in integrable systems exhibits a noticeable scientific advantage: it can be expressed in terms of the nonlinear modes of these systems. Whether the majority of the excitations in the system are breathers or solitons defines the properties of the turbulent state. In the two extreme cases we can call such states "breather turbulence" or "soliton turbulence." The number of rogue waves, the probability density functions of the chaotic wave fields, and their physical spectra are all specific for each of these two situations. Understanding these extreme cases also helps in studies of mixed turbulent states when the wave field contains both solitons and breathers, thus revealing intermediate characteristics.

DOI: 10.1103/PhysRevE.94.022212

I. INTRODUCTION

Turbulence is a common dynamical behavior of various systems in physics [1–4]. The wave turbulence theory [5,6] based on multiplicity of interacting waves provides a partially nonlinear description of fully developed turbulence. This is one of the challenging problems of modern theoretical physics. The wave turbulence theory has been applied to a diverse range of subjects including nonlinear optics, oceanography, plasma physics, and condensed matter physics. With some exceptions [6], this theory has not been applied to describe integrable systems. In particular, strongly nonlinear localized excitations such as breathers or solitons cannot be described by means of the weakly interacting wave turbulence theory. In this respect, the problem of integrable turbulence constitutes an important open issue of general interest. It cannot replace the theory of strong turbulence but may serve as an intermediate step for better understanding the concept of turbulence.

Integrable turbulence has attracted much attention in recent years [7–11]. The integrability of the governing equation provides us with the possibility to write down certain exact solutions for these systems. These solutions serve as elementary nonlinear modes of the system. Specifically, solitons and breathers can be mentioned as the modes that have a significant amplitude. This allows us to classify them as nonlinear modes. Radiation waves are also modes of the system comprising the chaotic background field but their role is less important because they have low amplitudes. The knowledge of the modes of integrable systems is the main advantage of dealing with them. Nonintegrable systems may reveal more complicated dynamics like "incoherent soliton states" [12]. However, these structures cannot be predicted directly from the initial conditions, thus making the analysis more involved even with periodic initial conditions.

Despite knowing these modes in explicit form, the complicated chaotic motion that involves a multiplicity of them interacting in a generally irregular way still remains an unsolved problem. Integrable turbulence can be analyzed mainly using numerical simulations [7,8], although the knowledge of involvement of nonlinear modes in this process can be useful [9]. The simplest chaotic pattern is formed when a multiplicity of solitons of different amplitudes move in all possible directions. Their collisions with well defined rules produce the points of high amplitude in the chaotic field. Such pattern can be called "soliton turbulence" [11,13,14].

An interesting situation arises when the chaotic motion starts with a continuous wave (cw) perturbed by a random component [7–9]. In our recent work [9], we have found that the resulting chaotic dynamics is caused not only by solitons. Breathers and their interactions are also involved into the dynamics. In the general case, the chaotic dynamics is defined by the relative number of solitons and breathers that are excited at the beginning of the process.

Clearly, the presence of the cw component in the initial conditions leads to the excitation of breathers through modulation instability. The competing process is the excitation of solitons which happens when the initial noise level is increased. A greater number of solitons in comparison to breathers results in a greater probability of generating rogue waves. This leads to the elevated tails of the probability density function (PDF) of the chaotic wave field [9]. A question arises: can we detect the presence of breathers and solitons measuring the physical spectra of these chaotic fields? The spectrum is one of the most common measurements that can be easily done experimentally both in optics and for oceanic waves. Our present work provides a detailed answer to this question and gives an elaborate description of the processes of excitation of solitons and breathers within the integrable turbulence.

II. MODEL

A classical example of integrable turbulence is based on the nonlinear Schrödinger equation (NLSE) [7–9] which is an ubiquitous equation used to describe nonlinear dynamical systems, such as nonlinear waves in optics [15–17], ocean gravity waves [18,19], Bose-Einstein condensates [20,21], waves in plasmas [22,23], and many others. Such universality makes the results obtained in one discipline applicable, with some adjustments, to other fields [24].

Despite being one of the simplest among the nonlinear partial differential evolution equations, the NLSE has provided

us with a deep understanding of how the nonlinear dynamical world operates. Importantly, it is a unique equation that combines particle and wave properties in the same description. Namely, particles in the form of solitons and waves in the form of carrier oscillations are contained in the same solutions.

Another significant property of the NLSE is its integrability [25]. This is a unique property of a selected class of nonlinear evolution equations. Integrability allows us to find solutions of this equation. More generally, it provides us with an opportunity to make a deeper analysis of what happens in wave evolution, not only in simple cases like one-soliton solution, but even in such a complicated situation as the turbulent motion. The inverse scattering technique (IST) is the main tool that can be used for at least a qualitative analysis of the phenomenon that we call "integrable turbulence." With this aim in mind, we start with writing the nonlinear Schrödinger equation in a dimensionless form:

$$i\psi_\xi + \tfrac{1}{2}\psi_{\tau\tau} + |\psi|^2\psi = 0, \tag{1}$$

where ξ is the evolution variable, τ is the transverse variable, and ψ is the envelope of the function describing the physical field of interest.

As with any other evolution equations, the dynamics described by Eq. (1) is completely determined by the initial conditions. Thus, here, we are operating with the so-called deterministic chaos. However, in contrast to chaos in systems with a finite number of degrees of freedom such as the logistic map [26], the Lorenz model [27,28], or the Hénon-Heiles system [29], chaos in systems with an infinite number of degrees of freedom, including Eq. (1), is governed by different principles. Some concepts developed for simpler systems such as strange attractor, period doubling, etc. may be further broadened and applied to special solutions of systems with an infinite number of degrees of freedom [30]. However, we stress that these concepts can only be applied to specific cases, for example, when dealing with localized solutions [30]. Such solutions can be characterized by one or two evolving parameters, say, soliton amplitude and width. This trickery effectively reduces the number of degrees of freedom in the system that we are operating with. On the other hand, the chaotic motion in systems with an infinite number of degrees of freedom comprises a whole new world which acquires completely new features. One of these features is the presence of rogue waves which are either doubly localized solutions of nonlinear partial differential equations [31] or high amplitude peaks created by the collision of breathers or solitons and mutual collisions between them [32]. The rogue waves obviously do not have analogs in the case of low dimensional systems such as the logistic map.

Dealing with deterministic chaos in such systems requires a special approach to the initial conditions. Two initial conditions even having the same set of parameters of a chaotic function lead to different dynamics along the evolution variable. They could be exponentially diverging in the corresponding infinite-dimensional phase space. However, it is not the distance between these diverging trajectories that is the main point of interest as in the Lorenz model. Consequently, we do not introduce the Liapunov exponent here. A better approach is to use a variety of initial conditions to generate many realizations of chaotic dynamics. Averaging their characteristic parameters provides us with the most likely pattern of chaos that can be observed in experiments.

III. INITIAL CONDITIONS

Following our previous work [9], we use the initial conditions in the form of a constant background perturbed by a random function:

$$\psi(\tau,0) = \frac{1}{\sqrt{Q}}[1 + \mu f(\tau)], \tag{2}$$

where $f(\tau)$ is a complex function, with its real and imaginary parts being two independent Gaussian distributed and Gaussian correlated random functions. They are characterized by the same variance $\sigma_f^2 = 1$, same zero mean values $\langle f\rangle = (0,0)$, and same correlation length L_c. Once μ and $f(\tau)$ are given, the factor Q

$$Q = \frac{1}{T}\int_0^T |1 + \mu f(\tau)|^2 d\tau, \tag{3}$$

is used to normalize the mean value of the field intensity to unity. Here T is the period of our numerical grid.

We have solved Eq. (1) with initial conditions (2) using a standard split step Fourier method. Our numerical method restricts us to use periodic boundary conditions in τ. Thus the initial conditions are chaotic only within this period. The larger the period, the closer are the results to the case of a chaotic field without boundaries. For this reason, we always deal with long periods. We used different step sizes and various periods, T, to make sure that our results are free of numerical artifacts.

The variation of the coefficient μ allows us to select the desired standard deviation for the function ψ and therefore for the initial field intensity $|\psi(\tau,0)|^2$, to which we shall refer from now on as $\sigma = \sigma(0)$, the initial standard deviation of the field intensity distribution. Namely,

$$\sigma(0) = \sqrt{\langle I(0)^2\rangle - \langle I(0)\rangle^2}, \tag{4}$$

where

$$\langle I(\xi)^n\rangle = \frac{1}{NT}\sum_{i=1}^{N}\int_0^T |\psi_i(\tau,\xi)|^{2n} d\tau,$$

while N is the number of realizations, typically one thousand. Roughly speaking, $\sigma(0)$ and the initial $L_c = L_c(0)$ give us the estimates of the mean height and the mean width of the waves in the initial wave field, respectively.

As it was clearly demonstrated in Ref. [9], integrable turbulence is characterized by the nonlinear modes of the system that we are dealing with. These are solitons, breathers, and small amplitude radiation waves. Their numbers, once the elementary modes are created, i.e., once the initial conditions are chosen, do not change during evolution. This is one of the fundamental results of the inverse scattering technique (IST) [25]. And it is a mere manifestation of the fact that the chaotic dynamics in an integrable system is completely deterministic and entirely defined by the initial conditions. Each individual initial condition contains a fixed number of modes. These numbers vary when choosing one random function $f(\tau)$ or another. However, the average number of excitations is fixed by the initial parameters μ (that fixes σ) and L_c.

There are three major mechanisms that contribute to the formation of the chaotic wave field. One is modulation instability (MI) that is responsible for the generation of breathers, the second one is the motion of solitons in all possible directions, and the third one is the interference pattern of the large number of small amplitude radiation waves. All three mechanisms contribute to the turbulent wave field of mixed type. As it was found in [9], initial conditions with small σ generate mainly Akhmediev breathers (ABs). At larger σ, both ABs and solitons are generated. At the largest σ, mainly solitons with various velocities result from the chaotic initial conditions. These nonlinear modes with high amplitudes are always located in the sea of small amplitude radiation waves.

IV. EIGENVALUES OF THE IST

Breathers that appear as a result of modulation instability are mostly excited when μ is small or, equivalently, when the parameter σ is small. In order to show this, we have calculated the IST eigenvalues for several initial conditions the same way as it was done in [9]. Figure 1 shows the IST eigenvalues, λ, calculated for 10 realizations of the function $f(\tau)$ in Eq. (2). In particular, Fig. 1(a) shows the results for $\sigma = 0.05$, while Fig. 1(b) shows the results for $\sigma = 0.1$. When $\psi(\xi = 0,\tau) =$ const, i.e., for $\mu = 0$, all eigenvalues must be purely imaginary, i.e., located along the vertical axis, and its imaginary part must be less than 1. They correspond to ABs. Small deviations of σ from zero leave them practically on the imaginary axis. This is clearly seen in Fig. 1(a). Small chaotic deviations from the imaginary axis can be observed in Fig. 1(b) for the higher value of $\sigma = 0.1$. We can also notice that, for $\sigma = 0.1$, the imaginary part of some eigenvalues exceed slightly $+i$. This part of the IST spectrum may correspond to the Kuznetsov-Ma solitons (solitons on a finite background) [33]. At the same time, a multiplicity of eigenvalues appear close to the real axis. These correspond to small amplitude radiation waves. For the values of σ smaller than 0.05, the eigenvalue distribution is practically the same as in Fig. 1(a). Moreover, for these small values of σ, the influence of the correlation length L_c is negligible.

The upper limiting point $\lambda = i$ in the IST spectrum corresponds to the Peregrine breather [34,35]. It has a peak amplitude of 3 which is the maximum possible value for breathers. The eigenvalues located below the point $\lambda = i$ on the imaginary axis correspond to ABs, which have lower amplitudes. They continuously occupy the whole interval of unstable frequencies inside the modulation instability gain curve. Discreteness in Fig. 1 is due to the use of periodic boundary conditions in our numerical scheme. Ten realizations with different numerical periods are used in each case to get a denser distribution of eigenvalues along the vertical axis. The same effect could be obtained by increasing the number of mesh points and T. In the eigenvalue problems, we are limited numerically to use no more than 16384 mesh points. In most cases we used 8192 points and verified that the results were virtually identical with the case of 16384 points.

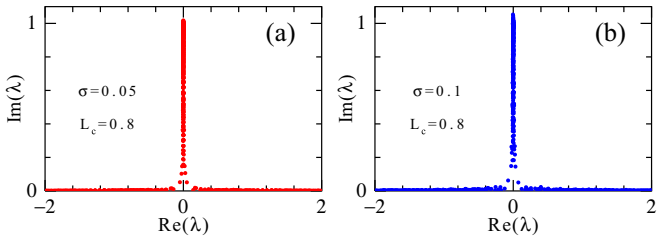

FIG. 1. Set of complex eigenvalues of the IST, λ, calculated for ten realizations of the initial conditions given by Eq. (2) with (a) $\sigma = 0.05$ and (b) $\sigma = 0.1$. As the eigenvalues appear in complex conjugate pairs, only the upper half of the complex plane is shown in each panel. For these values of σ, the value of L_c hardly makes any difference.

Modulation instability generates breathers with all possible frequency components within the instability band, i.e., for ω in the interval $[-2,2]$. In other words, all eigenvalues below the point i are excited with equal probability. Similar to solitons, individual breathers, once excited, propagate along the ξ axis indefinitely. Moreover, their interaction is similar to the interaction of solitons. Breathers collide but do not change their parameters except for a phase shift along the propagation direction. This can be seen from the exact solutions for the collision of breathers [36]. A general scheme for analyzing the collision of N breathers has been given in Refs. [37,38]. For a finite number of breathers, all results could be presented in analytical form. When dealing with chaotic wave fields, we assume the presence of an infinite number of breathers with slight variations of initial conditions for each of them. In this case, a similar analysis of their interaction based on general rules [38] may provide a qualitative description of the wave patterns.

The ideal breather grows exponentially from a constant background, reaches its maximum amplitude, and decays, also exponentially at $\xi \to +\infty$. The exponential growth-decay cycle of each breather with the growth rate of the MI given by $\delta = \omega\sqrt{1-\omega^2/4}$ depends on its transverse frequency ω. Thus the location of the maximum amplitude along the ξ axis varies significantly from one breather to another. For smaller δ, this point may be shifted far away from the initial point $\xi = 0$. On the other hand, for a finite initial perturbation, each AB starts with a small but finite amplitude. It also depends on the initial chaotic field variations, i.e., on σ. Moreover, initial amplitudes are also chaotic due to the uncertainty of a particular frequency component in the chaotic function $f(\tau)$.

In terms of nonlinear dynamics theory, the ideal AB starts from a saddle point and ends at another saddle point as explained in [39]. Due to the exponential tails, this trajectory requires an infinite amount of time for the whole cycle of evolution. On the contrary, the breather created from the chaotic initial conditions starts from one of the nearby hyperbolic orbits. These orbits are periodic rather than heteroclinic as shown in Fig. 1 of [39]. Periods of these orbits are finite. They are highly sensitive to the deviations from the heteroclinic orbits. Consequently, the points in ξ where each individual breather reaches its maximum move closer to the initial point $\xi = 0$. Moreover, the points of maxima are repeated periodically. Their location depends on the growth rate δ as well as on the initial deviation from the heteroclinic orbit. The evolution of these periodic breathers amended by collisions continues indefinitely. Collisions add a phase shift to each AB [36,37] otherwise leaving them intact.

All breathers excited from the initial condition (2) comprise a composite N-breather solution [38], with N being the total number of breathers. As explained above, the period of the evolution along the ξ variable varies significantly from one AB to another. Moreover, these periods are incommensurate. Thus their nonlinear superposition leads to a continuous chaotic dynamics. Only the initial stage that starts from a cw has a distinctive exponential growth dominated by the maximal growth rate of the modulation instability. Once all breathers are excited, the rest of the evolution reaches a "steady" chaotic state with certain deviations around its mean value. The starting point $\xi = 0$ is unique in the sense that all breather modes start here from small perturbations simultaneously. This state never repeats due to the multiplicity of modes and because their periods along ξ are incommensurate.

This process is confirmed by our numerical simulations. We calculated the changes of the standard deviation $\sigma(\xi)$ along the axis ξ for several initial values of σ. Each curve in Fig. 2 shows the ξ dependence of the standard deviation of the field intensity calculated for one thousand realizations with the same initial statistical parameters. The period, T, of each realization was taken to be 800, and sampled with 131072 points. Nine initial values of σ are used while L_c is kept constant (=1.2). The horizontal scales used in the left and in the right halves of the figure are different to show more clearly the initial variations and the convergence of each $\sigma(\xi)$ curve to a stationary value.

The lowest (short dashed magenta) curve in Fig. 2 shows the result for the value of $\sigma = 0.075$. For this smallest σ, nearly all IST eigenvalues correspond to ABs as can be seen from Fig. 1. Thus this case illustrates the "breather turbulence." The initial growth of σ is exponential as expected from the above description with the maximal growth rate of MI. After reaching its first maximum amplitude the AB with the maximum growth rate returns to its initial stage. Correspondingly, this curve shows a few oscillations related to the periodic evolution of this component. The ABs with other frequencies also grow although with a slower rate. When most of the ABs are excited, the curve shows the signs of the "steady" chaotic state.

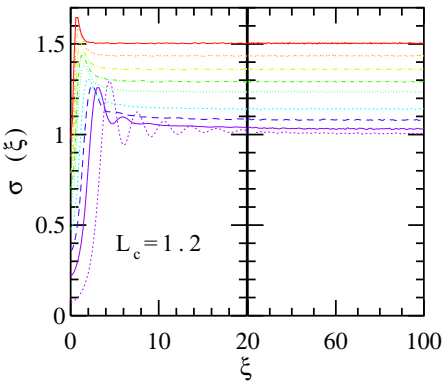

FIG. 2. Evolution of the standard deviation of the field intensity for nine initial values of σ (namely, from the lowest curve to the highest: $\sigma = 0.075, 0.22, 0.36, 0.48, 0.62, 0.70, 0.79, 0.88$, and 0.98) and correlation length $L_c = 1.2$. Each curve converges to a different steady value that corresponds to a different chaotic state that lasts indefinitely. The value of σ at $\xi \to \infty$ depends on the initial value $\sigma(0)$. Note that the horizontal scales to the left and to the right of the point $\xi = 20$ are different.

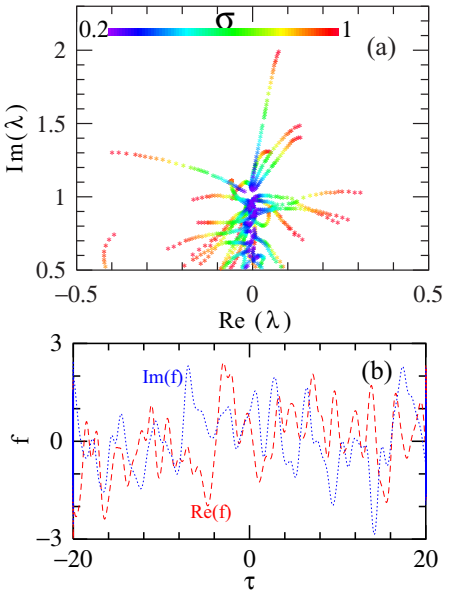

FIG. 3. (a) IST eigenvalues found in the interval: $-0.5 < \mathrm{Re}(\lambda) < 0.5$, $\mathrm{Im}(\lambda) > 0.5$ for a fixed function $f(\tau)$ and variable μ. A small portion of the function $f(\tau)$ is shown in (b). Each color in (a) represents a certain value of σ (or μ). The minimal value of σ used here is 0.2. Smaller σ leaves the eigenvalues on the imaginary axis or very close to it. The correlation length used for these calculations is $L_c = 0.76$.

The increase of σ pushes the IST eigenvalues off the imaginary axis. One example of the eigenvalue relocations as the initial σ increases is shown in Fig. 3(a). A portion of the function $f(\tau)$ used for these calculations is shown in Fig. 3(b). It is fixed but μ increases continuously together with the initial σ. Consequently, the IST eigenvalue relocation is also continuous and specific for this case. The eigenvalues move along certain trajectories in the complex plane which are determined by the function $f(\tau)$. Importantly, they all move away from the imaginary axis. Different functions $f(\tau)$ result in similar shifts of the eigenvalues but along different trajectories. As a result, for many realizations of the random function $f(\tau)$ the IST eigenvalues would be dispersed randomly on the complex plane. The region that they occupy in the complex plane becomes wider when the initial σ increases.

To summarize, for small σ (the smallest one considered here is 0.2), the IST eigenvalues shown by magenta stars are located on the imaginary axis or very close to it. Most of them are located below the point i, indicating that the nonlinear modes are mainly ABs. The growth of σ disperses the eigenvalues away from the imaginary axis and above the value i. The latter correspond to solitons with a range of amplitudes and velocities. The net result of increasing σ is the split of breathers into solitons with each having individual amplitude and velocity. For better resolution, Fig. 3(a) shows only the eigenvalues contained within the interval of real parts $[-0.5, 0.5]$ and with imaginary parts above 0.5.

V. CONVERSION OF BREATHER TURBULENCE INTO SOLITON TURBULENCE

Larger values of σ result in practically no eigenvalues left exactly on the imaginary axis. The set of eigenvalues obtained for 30 realizations of the random function $f(\tau)$ with fixed L_c and μ (σ) is shown in Fig. 4. In order to see more clearly the randomness of the eigenvalues, two specific realizations are singled out and represented by red triangles and blue circles, respectively. Increasing the number of realizations results in denser filling of the complex plane around the real and imaginary axes.

Practically all eigenvalues in Fig. 4 correspond to solitons rather than breathers. Their amplitudes are twice the imaginary part of the eigenvalue. Solitons gain velocity which is defined by the real part of the complex eigenvalue. Moreover, these solitons are located on a background that consists of a sea of radiation waves. Thus, when the perturbation is comparable to the amplitude of the initial cw, the continuous spectrum of breathers is replaced by the spectrum of solitons. Figure 4 shows clearly such a transformation, when compared with Fig. 1.

Therefore, as σ increases, the number of breathers decreases, whereas the number of solitons increases. Moreover, the amplitudes and velocities of solitons also grow. The chaotic dynamics is then caused by the collisions between breathers, between solitons, and between breathers and solitons. At the highest values of σ, all breathers are completely destroyed and the chaotic behavior is fully originated by the solitons and their collisions. Thus the increase of σ causes the transition from "breather turbulence" to "soliton turbulence."

Within the soliton turbulence, most of the nonlinear modes that lead to high amplitude peaks are solitons and their collisions. As we can see from Fig. 4, the imaginary part of the eigenvalues can be higher than 1 and reach a value of almost 2. Thus the soliton amplitudes may reach a value close to 4. This is higher than the maximal amplitudes that breathers can reach. In contrast to breathers, solitons do not experience an exponential growth. They are generated practically from the very beginning of the evolution at $\xi = 0$. Therefore, the larger the initial σ, the sooner the stationary value of σ is reached. This can be seen from Fig. 2. Still existing transition to the soliton turbulence regime at higher σ is related to the process of

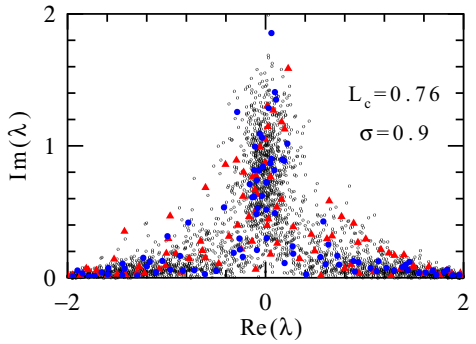

FIG. 4. IST eigenvalues, marked by small circles, obtained for 30 realizations with $\sigma = 0.9$ and $L_c = 0.76$. Two particular realizations among them are singled out by red triangles and blue circles.

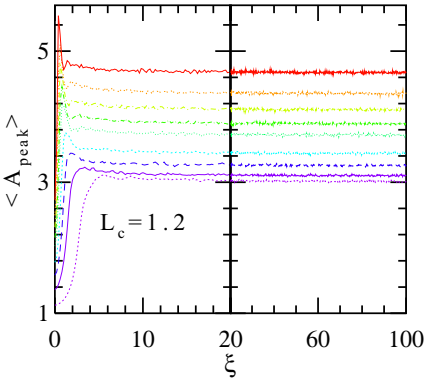

FIG. 5. Evolution of the mean highest amplitude obtained by averaging the peak amplitude over the same thousand of realizations as in Fig. 2. The mean maximum in all cases is above the value 3 which is the amplitude of the Peregrine solution [35].

separation of solitons and the radiation waves. The background consisting of small amplitude radiation waves does exist at all values of σ.

The convergence to the limiting state of turbulence can be further seen from Fig. 5, where we show the evolution of the average peak amplitude. Each curve is obtained by averaging the peak amplitudes for one thousand realizations at each point ξ. The color codes and the line styles used here are the same as in Fig. 2. The curves correspond to the same initial values of $\sigma(0)$. It is noticeable that, for all initial $\sigma(0)$, the stationary value of the mean peak amplitude is above 3. The latter is the peak amplitude that corresponds to the Peregrine soliton [35]. The plots in Fig. 5 confirm once again that the limiting chaotic state reached at $\xi = 20$ stays roughly the same at $\xi = 100$ and continues indefinitely along the ξ axis. There is no return back to the initial state at any ξ. Any parameter of the chaotic state calculated at $\xi = 100$ can be considered as the limiting value roughly valid at any $\xi > 100$.

VI. PROBABILITY DENSITY FUNCTIONS

Just as any other measurable parameter of the chaotic state, the probability of having certain maximal intensities also saturates and reaches a limiting value at $\xi = 100$. Then the corresponding probability density function can also be considered to remain unchanged during the following evolution beyond $\xi = 100$ up to very high values of ξ. These limiting curves calculated for the same set of initial σ values as in Figs. 2 and 5 are presented in Fig. 6. The larger the initial σ, the higher is the tail of its corresponding PDF. This is expected as the increase of σ leads to the generation of solitons with increased amplitudes and velocities. Thus the intensity at their collision points and the number of collisions are also higher.

VII. INFLUENCE OF THE CORRELATION LENGTH

The parameter σ is not the only one that controls the chaotic function in the initial conditions. The second important parameter is the correlation length L_c. While σ provides an estimate of the mean height of the chaotic wave field, the correlation length L_c gives us an estimate of the mean width

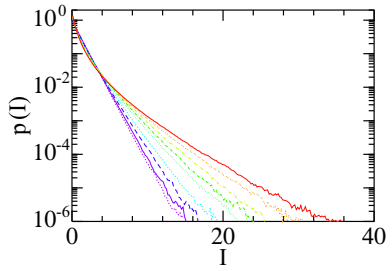

FIG. 6. Comparison of the PDF curves obtained at $\xi = 100$ averaged over a thousand of realizations for the same values of the initial σ (0.075, 0.22, 0.36, 0.48, 0.62, 0.70, 0.79, 0.88, and 0.98) and correlation length $L_c = 1.2$ as in Fig. 2. The probability of extreme events at any given I steadily increases with the value of the initial σ adding up to at least two orders of magnitude elevation within the given range of σ.

of the chaotic field variations. In other words, it shows how smooth or sharp are the initial field variations.

Numerical simulations show that at small σ the correlation length does not influence the results. This happens because the ABs are not influenced by this parameter. The whole dynamics is determined by modulational instability. The IST eigenvalues in Fig. 1 are located on the imaginary axis no matter what is the value of L_c. Thus the whole AB dynamics remains the same as explained above. On the other hand, the excitations of solitons depends on the details of the initial perturbation function. In order to evaluate its influence, we have calculated the IST eigenvalues for one realization of the chaotic function with fixed high $\sigma = 0.84$ and a correlation length that increases continuously from 0.5 to 1.0. The results are shown in Fig. 7(a). As before, for the sake of clarity, we

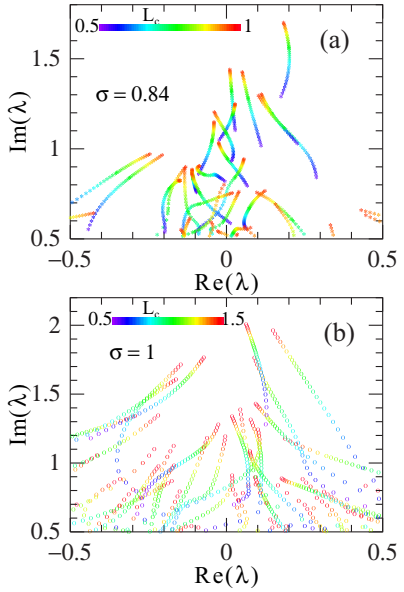

FIG. 7. (a) Relocation of the IST eigenvalues on the complex plane for a single realization of the perturbation function with constant $\sigma = 0.84$ and L_c changing from 0.5 to 1.0. (b) Relocation of the eigenvalues for the case when the initial cw component is absent (thus $\sigma = 1.0$). The value of L_c here varies from 0.5 to 1.5.

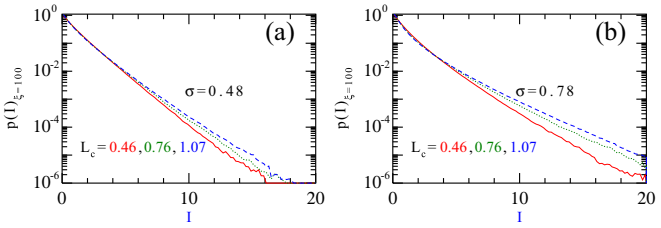

FIG. 8. Probability density functions calculated at $\xi = 100$ for (a) $\sigma = 0.48$, (b) $\sigma = 0.78$, and for three different values of L_c. Namely, the solid red curves in each panel correspond to $L_c = 0.46$, the dotted green curves to $L_c = 0.76$, and the dashed blue curves to $L_c = 1.07$.

show only those eigenvalues whose imaginary part is greater than 0.5 and its real part is in the interval $[-5,5]$. We can see that the IST eigenvalues are continuously relocating on the complex plane when L_c is changing, with a clear tendency to increase its imaginary part and decrease the absolute value of its real part, as L_c increases. Similar results are obtained if the cw is removed from the initial conditions. This case is shown in Fig. 7(b). Here, $\sigma = 1$ and we deal with an even greater variation of L_c, namely from 0.5 to 1.5. The general tendency is the same in both cases: the soliton amplitudes increase while their velocities decrease.

For most of the eigenvalues, but not for all of them, the absolute value of its real part decreases when increasing L_c. This means that the soliton velocities change and in average they decrease. However, the most dramatic effect that the change of L_c makes is the systematic increase of the imaginary part of the eigenvalues. This means that the soliton amplitudes become higher for higher L_c. This must lead to the increase of the rogue wave amplitudes. This conclusion is confirmed by the numerical simulations. On the other hand, the decrease of the soliton velocities reduces the number of their collisions. This second effect tends to partially compensate the growth of the amplitudes. Thus the effect of changing L_c is weaker than that of changing σ.

Figure 8 shows the probability density functions calculated for various L_c. For small $\sigma = 0.1$, all three PDF curves are practically the same. This case is not shown here. However, for higher values of σ, namely 0.48 and 0.78, the tails of the curves are more elevated for higher L_c. This can be seen from Figs. 8(a) and 8(b). Our detailed calculations show that the difference in the rogue wave amplitudes can reach two orders of magnitude when increasing L_c up to 1.8.

Thus the integrable turbulence provides us with two parameters in the initial conditions that allow us to control the number of extreme events in the chaotic wave field. Choosing higher values for each of them allows us to increase the amplitudes of rogue waves by orders of magnitude. Thus the control can be very efficient.

VIII. PHYSICAL SPECTRA

One of the main characteristics of a chaotic wave field measured in experiments is its physical spectrum. Spectra are commonly measured in optics and they are also useful in water wave studies [40]. When other parameters of the chaotic wave field are stabilized, the spectrum also gets a roughly

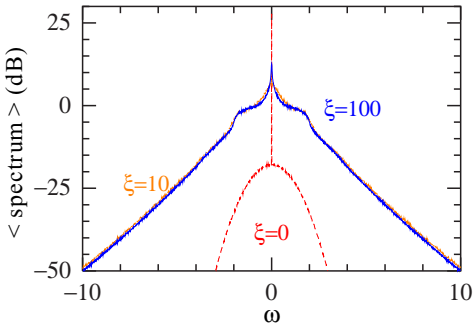

FIG. 9. (a) Average initial spectrum (red), the average spectrum at $\xi = 10$ (orange), and at $\xi = 100$ (blue) for $\sigma = 0.1$. For this initial level of noise, the spectrum hardly changes starting from $\xi = 10$, and the dependence on L_c is scarce. Modulation instability leads to the amplification of the central part of the spectrum within the MI gain band, i.e., for ω in the interval $[-2,2]$.

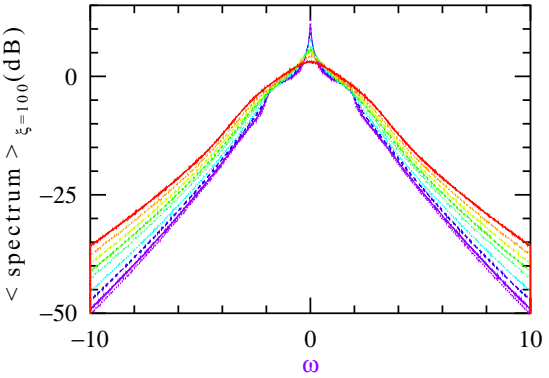

FIG. 10. Averaged spectrum at $\xi = 100$ for the same values of the initial σ and correlation length $L_c = 1.2$ as in Fig. 2. The color code and the styles of the curves here correspond to the same values of σ as in Figs. 2, 5, and 6.

fixed shape. One example is shown in Fig. 9. Spectra in this figure are averaged as in the previous cases over one thousand realizations. Here, the red dashed curve corresponds to the average initial spectrum, while the blue curve is the average spectrum at $\xi = 100$. It is almost the same spectrum as at $\xi = 10$ shown by the orange solid curve confirming that the steady spectrum is quickly reached. This specific shape of the spectrum is observed when σ is small. Namely, $\sigma = 0.1$ in this particular case. This value of σ corresponds to "breather turbulence" as explained above. Consequently, this shape of the spectrum is also characteristic for the breather turbulence. This spectrum is hardly influenced by the value of L_c.

The spectrum of the initial conditions shown in red in Fig. 9 consists of a central peak due to the cw component and a parabolic background due to the Gaussian correlated noise component. The central peak decreases in evolution spreading its energy into the multiplicity of sidebands within the MI instability band. All frequency components are amplified due to the MI. The growth rate for each frequency ω is given by $\delta = \omega\sqrt{1-\omega^2/4}$. This growth rate is real within the interval of frequencies $[-2,2]$. These frequencies are the only ones amplified at the beginning of the propagation. Correspondingly, the spectrum in Fig. 9 has an elevated part exactly in this interval resulting in the characteristic "onion dome" shape. This is an additional confirmation that most of the modes in the chaotic wave field are ABs. The tails of the spectrum also grow from a parabolic shape to the universal triangular shape [41] taking energy from the central peak through cascades of four wave mixing processes. Despite the significant growth, the total energy in the tails remains much smaller than in the central region within the MI interval. The central part of the spectrum has a power-law shape due to the homogeneous presence of all components of the breather spectrum within this region.

Increasing σ causes a gradual transformation from the breather turbulence to the soliton turbulence. The physical spectra change their shape accordingly. A sequence of such transformations is shown in Fig. 10. The onion dome shape is still in place for the lower values of σ up to 0.2 but gradually diminishes at higher σ showing the replacement of breathers by solitons. This specific shape completely disappears at the values of σ close to 0.9 indicating that most, if not all, high amplitude modes are now solitons. The red dashed curve in Fig. 10 is the ultimate example of the transformed spectrum. This shape corresponds to solitons moving with nonzero velocities in all possible directions. This leads to the tails of this spectrum being elevated in comparison to the spectral tails in the breather case.

Very roughly, the spectrum of the field in the case of soliton turbulence can be estimated in the assumption that it is produced as a superposition of the spectra of the individual solitons. In doing this, we ignore soliton collisions. We consider the density of solitons to be low so that the number of collisions are much smaller than the number of solitons. Collisions transform the spectrum of individual solitons and may distort the overall spectrum. To be specific, soliton profiles are given by the expression $2b\,\mathrm{sech}(2b\tau)\exp(i2a\tau)$, where a and b are the real and imaginary parts of the IST eigenvalues. The corresponding Fourier spectrum of these solitons is given by the expression $\pi\,\mathrm{sech}[\pi(w-2a)/2b]$. In the accepted approximation, the square of the sum of the individual soliton Fourier transform is the overall spectrum of the soliton turbulence.

In order to obtain the experimentally observable spectrum, these spectra must be averaged over the number of realizations. In these simulations, we used 26 realizations. Each realization consisting of 8192 points sampling the temporal interval $[0,100]$. The results are shown in Fig. 11. Each curve in this figure is for a specific correlation length: dotted green ($L_c = 1$), dashed blue ($L_c = 2$), and solid red ($L_c = 0.5$). The spectra reveal some oscillations in the tails for the smallest L_c. This is due to the eigenvalues with imaginary parts being close to zero and due to the insufficient number of data. Otherwise, the qualitative features of the central parts of the curves are the same as for the red and orange curves in Fig. 10. A more precise comparison shows deviations due to the fact that soliton collisions and small amplitude radiation waves have been ignored in the estimates.

In contrast to the case of the breather turbulence, the spectra of the soliton turbulence strongly depend on the correlation length L_c. This happens because the amplitude and velocity distribution of solitons in the chaotic field strongly depends

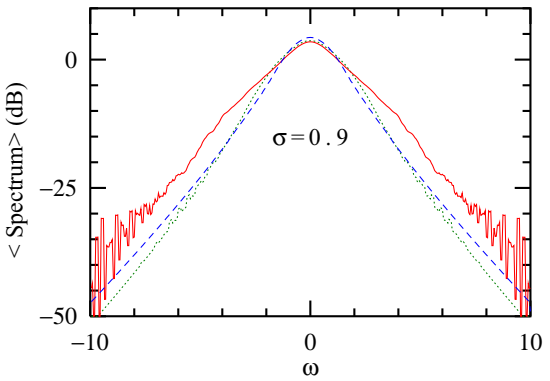

FIG. 11. Estimated spectra of the soliton turbulence for $\sigma = 0.9$ and correlation length $L_c = 1$ (dotted green curve), $L_c = 2$ (dashed blue curve), and $L_c = 0.5$ (solid red curve).

on the correlation length. As a result, the spectra also depend on L_c. This can be seen in Fig. 11. In order to demonstrate this dependence more clearly, we made simulations removing completely the breather part of the chaotic field. Namely, in these simulations, we omit the cw in the initial conditions leaving only the chaotic function $f(\tau)$. μ is then irrelevant due to the normalization factor Q, and the variance is therefore imposed to be unity. The results are shown in Fig. 12.

Wave fields with initial small correlation length, such as $L_c = 0.19$, show a wide spectrum with low amplitude components that do not change on propagation [see Fig. 12(a)]. The spectrum at $\xi > 100$ is almost an exact copy of the initial spectrum. This indicates that the spectral components correspond to small amplitude radiation waves, and their propagation is linear. Initial parabolic spectrum stays nearly intact during the whole evolution process. The chaotic field in this case does not contain solitons. The latter are the only nonlinear modes that have a potential to change the spectrum.

Increasing the correlation length to $L_c = 0.78$ in the initial conditions makes the initial spectrum narrower but raises the spectral components in the middle. The central part of the spectrum now reaches the zero level which is sufficient for turning on the nonlinearity and for generation of solitons. The resulting chaotic field is now a mixture of solitons and small amplitude radiation waves. Moreover, solitons may acquire velocity which is given by the real part of the IST eigenvalues shown in Fig. 4. The value of the velocity is directly proportional to the corresponding frequency component. This way, the energy is transported from the center of the spectrum to its tails. This process elevates the tails of the spectrum and depletes its middle part. This case is shown in Fig. 12(b). Similar elevation of the tails of the initially Gaussian spectrum has been observed numerically and experimentally in Ref. [6]. However, the authors of [6] mostly concentrated on the case of fiber with normal dispersion when breathers and bright solitons do not exist. Clearly, the physical reasons for the spectrum widening in that case are different.

Further increase of the correlation length to $L_c = 1.8$ elevates the central part of the spectrum above the zero line at the expense of the tails. This, in turn, increases the number of solitons, their amplitudes, and modifies the distribution of their velocities, thus elevating the tails of the spectrum even

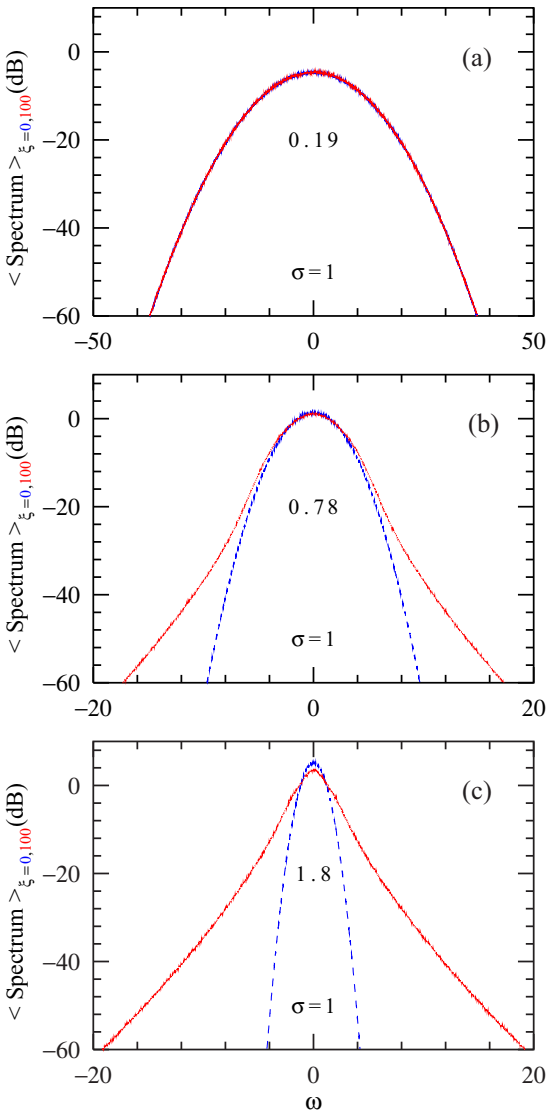

FIG. 12. Averaged initial spectra (blue dashed curve) and the averaged spectra at $\xi = 100$ (red solid curve), when the initial condition does not contain cw. The value of $\sigma = 1$ is the same for all panels. The correlation length $L_c =$ (a) 0.19 (b) 0.78, and (c) 1.8.

higher. This case is shown in Fig. 12(c). The spectrum widens further due to the increased energy transport by solitons from the central area of the spectrum to its tails.

IX. CONCLUSIONS

In this work, we have found two regimes of chaotic wave generation that we call breather turbulence and soliton turbulence. Which one is generated depends very much on the initial conditions. There are also intermediate cases when both breathers and solitons contribute to the chaotic pattern on an equal basis. For an integrable system, the initial conditions determine the set of IST eigenvalues. Their location on the complex plane is crucial for further evolution of the wave field. Numerical simulations provide the distribution of IST eigenvalues on the complex plane that allows us to analyze the follow up dynamics.

We have found that two parameters of the initial chaotic functions are essential to fix the number of rogue waves in the resulting chaotic wave field: σ and the correlation length L_c. The parameter σ influences the relative number of breathers and solitons in the resulting chaotic wave field while the parameter L_c mainly influences the amplitudes of the solitons. Both mechanisms increase the amplitudes of rogue waves. Namely, the increase of σ leads to the increase of the number of solitons, while the increase of L_c leads to the increase of soliton amplitudes but does not influence the breathers. These values, in turn, influence the measurable parameters of the chaotic wave state, such as the probability density functions and its physical spectra. The relation between the parameters of the initial conditions and the external measurable ones is essential for experimental studies of the chaotic wave states.

An additional insight on the breather versus soliton turbulence can be provided with the analysis of the Hamiltonian, H, for the chaotic solutions. This approach has been initiated by Connaughton *et al.* in [42]. As the authors of [42] noticed, the Hamiltonian plays the role of an effective "temperature" for the microcanonical statistical ensemble. Being a conserved quantity, the Hamiltonian characterizes the state of the system during its whole evolution in ξ. Although we have made the calculations of H for all cases above, these data require a deeper analysis than we presently are able to provide and we leave these studies for a separate publication.

ACKNOWLEDGMENTS

The authors acknowledge the support from the Volkswagen Stiftung. The work of JMSC was also supported by MINECO under Contract No. TEC2015-71127-C2-1-R, and by C.A.M. under Contract No. S2013/MIT-2790. N.D. and N.A. acknowledge support of the Australian Research Council (Discovery Project No. DP140100265).

[1] S. Wabnitz, Optical turbulence in fiber lasers, Opt. Lett. **39**, 1362 (2014).
[2] K. Hammani, B. Kibler, C. Finot, and A. Picozzi, Emergence of rogue waves from optical turbulence, Phys. Lett. A **374**, 3585 (2010).
[3] M. Conforti, A. Mussot, J. Fatome, A. Picozzi, S. Pitois, C. Finot, M. Haelterman, B. Kibler, C. Michel, and G. Millot, Turbulent dynamics of an incoherently pumped passive optical fiber cavity: Quasisolitons, dispersive waves, and extreme events, Phys. Rev. A **91**, 023823 (2015).
[4] J. C. Wyngaard, *Turbulence in the Atmosphere* (Academic Press, New York, 2010).
[5] A. C. Newell, S. Nazarenko, and L. Biven, Wave turbulence and intermittency, Physica D **152-153**, 520 (2001).
[6] P. Suret, A. Picozzi, and S. Randoux, Wave turbulence in integrable systems: nonlinear propagation of incoherent optical waves in single-mode fibers, Opt. Express **19**, 17852 (2011).
[7] D. S. Agafontsev and V. E. Zakharov, Integrable turbulence and formation of rogue waves, Nonlinearity **28**, 2791 (2015).
[8] P. Walczak, S. Randoux, and P. Suret, Optical Rogue Waves in Integrable Turbulence, Phys. Rev. Lett. **114**, 143903 (2015).
[9] J. M. Soto-Crespo, N. Devine, and N. Akhmediev, Integrable Turbulence and Rogue Waves: Breathers or Solitons?, Phys. Rev. Lett. **116**, 103901 (2016).
[10] P. Suret, R. El Koussaifi, A. Tikan, C. Evain, S. Randoux, Ch. Szwaj, and S. Bielawski, Direct observation of rogue waves in optical turbulence using time microscopy, arXiv:1603.01477v1 [physics.optics].
[11] A. Picozzi, J. Garnier, T. Hansson, P. Suret, S. Randoux, G. Millot, and D. N. Christodoulides, Optical wave turbulence: Towards a unified nonequilibrium thermodynamic formulation of statistical nonlinear optics, Phys. Rep. **542**, 1 (2014).
[12] A. Picozzi and J. Garnier, Incoherent Soliton Turbulence in Nonlocal Nonlinear Media, Phys. Rev. Lett. **107**, 233901 (2011).
[13] A. I. D'yachenko, V. E. Zakharov, A. N. Pushkarev, V. F. Shvets, and V. V. Yan'kov, Zh. Eksp. Teor. Fiz. **96**, 2026 (1989) [Soliton turbulence in nonintegrable wave systems, Sov. Phys. JETP **69**, 1144 (1989)].
[14] A. Costa, A. R. Osborne, D. T. Resio, S. Alessio, E. Chrivì, E. Saggese, K. Bellomo, and C. E. Long, Soliton Turbulence in Shallow Water Ocean Surface Waves, Phys. Rev. Lett. **113**, 108501 (2014).
[15] A. Hasegawa and F. Tappert, Transmission of stationary nonlinear optical pulses in dispersive dielectric fibers, I. Anomalous dispersion, Appl. Phys. Lett. **23**, 142 (1973).
[16] J. M. Dudley, F. Dias, M. Erkintalo, and G. Genty, Instabilities, breathers and rogue waves in optics, Nat. Photon. **8**, 755 (2014).
[17] S. Coulibaly, E. Louvergneaux, M. Taki, and L. Brevdo, Spatiotemporal wave-train instabilities in nonlinear Schrödinger equation: revisited, Eur. Phys. J. D **69**, 186 (2015).
[18] A. R. Osborne, *Nonlinear Ocean Waves* (Academic Press, New York, 2009).
[19] V. E. Zakharov, Stability of periodic waves of finite amplitude on the surface of a deep fluid, J. Appl. Mech. Tech. Phys. **9**, 190 (1968).
[20] E. P. Gross, Structure of a quantized vortex in boson systems, II Nuovo Cimento **20**, 454 (1961).
[21] M. Abida, C. Huepeb, S. Metensc, C. Nored, C. T. Phame, L. S. Tuckermand, and M. E. Brachete, Gross-Pitaevskii dynamics of Bose-Einstein condensates and superfluid turbulence, Fluid Dyn. Res. **33**, 509 (2003).
[22] B. P. Pandey, S. V. Vladimirov, and A. Samarian, Nonlinear waves in collisional dusty plasma, Phys. Plasmas **15**, 053705 (2008).
[23] S. M. Ahmed, M. S. Metwally, S. A. El-Hafeez, and W. M. Moslem, On the generation of rogue waves in dusty plasmas due to modulation instability of nonlinear Schrödinger equation, Appl. Math. Inf. Sci. **10**, 317 (2016).
[24] B. Kibler, A. Chabchoub, A. Gelash, N. Akhmediev, and V. E. Zakharov, Superregular Breathers in Optics and Hydrodynamics: Omnipresent Modulation Instability Beyond Simple Periodicity, Phys. Rev. X **5**, 041026 (2015).
[25] V. E. Zakharov and A. B. Shabat, Zh. Eksp. Teor. Fiz. **61**, 118 (1971) [Exact theory of two-dimensional self-focusing and one-dimensional self-modulation of waves in nonlinear media, J. Exp. Theor. Phys. **34**, 62 (1972)].

[26] R. M. May, Simple mathematical models with very complicated dynamics, Nature (London) **261**, 459 (1976).
[27] E. Lorenz, The problem of deducing the climate from the governing equations, Tellus **16**, 1 (1964).
[28] P. Bergé, Y. Pomeau, and Ch. Vidal, *Order within Chaos: Towards a Deterministic Approach to Turbulence* (John Wiley and Sons, New York, 1984).
[29] M. Hénon and C. Heiles, The applicability of the third integral of motion: Some numerical experiments, Astron. J. **69**, 73 (1964).
[30] J. M. Soto-Crespo and N. Akhmediev, Soliton as Strange Attractor: Nonlinear Synchronization and Chaos, Phys. Rev. Lett. **95**, 024101 (2005).
[31] N. Akhmediev, A. Ankiewicz, and M. Taki, Waves that appear from nowhere and disappear without a trace, Phys. Lett. A **373**, 675 (2009).
[32] S. Toenger, T. Godin, C. Billet, F. Dias, M. Erkintalo, G. Genty, and J. M. Dudley, Emergent rogue wave structures and statistics in spontaneous modulation instability, Sci. Rep. **5**, 10380 (2015).
[33] B. Kibler, J. Fatome, C. Finot, G. Millot, G. Genty, B. Wetzel, N. Akhmediev, F. Dias, and J. M. Dudley, Observation of Kuznetsov-Ma soliton dynamics in optical fibre, Sci. Rep. **2**, 463 (2012).
[34] V. I. Shrira and V. V. Geogjaev, What makes the Peregrine soliton so special as a prototype of freak waves?, J. Eng. Math. **67**, 11 (2010).
[35] B. Kibler, J. Fatome, C. Finot, G. Millot, F. Dias, G. Genty, N. Akhmediev, and J. M. Dudley, The Peregrine soliton in nonlinear fibre optics, Nat. Phys. **6**, 790 (2010).
[36] N. N. Akhmediev, V. M. Eleonskii, and N. E. Kulagin, Zh. Eksp. Teor. Fiz. **89**, 1542 (1985) [Generation of periodic trains of picosecond pulses in an optical fiber: Exact solutions, Sov. Phys. JETP **62**, 894 (1985)].
[37] N. Akhmediev and A. Ankiewicz, *Solitons, Nonlinear Pulses and Beams* (Chapman and Hall, London, 1997).
[38] N. Akhmediev, V. I. Korneev, and N. V. Mitskevich, Zh. Eksp. Teor. Fiz. **94**, 159 (1988) [N-modulation signals in a single-mode optical waveguide under nonlinear conditions, Sov. Phys. JETP **67**, 89 (1988)].
[39] N. N. Akhmediev and V. I. Korneev, Teor. Mat. Fiz. **69**, 189 (1986) [Modulation instability and periodic solutions of nonlinear Schrödinger equation, Theor. Math. Phys. **69**, 1089 (1986)].
[40] A. Chabchoub, S. Neumann, N. P. Hoffmann, and N. Akhmediev, Spectral properties of the Peregrine soliton observed in a water wave tank, J. Geophys. Res. **117**, C00J03 (2012).
[41] N. Akhmediev, A. Ankiewicz, J. M. Soto-Crespo, and J. M. Dudley, Universal triangular spectra in parametrically-driven systems, Phys. Lett. A **375**, 775 (2011).
[42] C. Connaughton, C. Josserand, A. Picozzi, Y. Pomeau, and S. Rica, Condensation of Classical Nonlinear Waves, Phys. Rev. Lett. **95**, 263901 (2005).